






Galaxy Zoo Builder: Four Component Photometric decomposition of Spiral Galaxies Guided by Citizen Science

TIMOTHY K. LINGARD ¹, KAREN L. MASTERS ², COLEMAN KRAWCZYK,¹ CHRIS LINTOTT,³ STEVEN BAMFORD,⁴
SANDOR KRUK ⁵, BROOKE SIMMONS ⁶, ROBERT SIMPSON,⁷ AND ROBERT C. NICHOL ¹

¹*Institute of Cosmology and Gravitation*

University of Portsmouth

Dennis Sciama Building

Burnaby Road

Portsmouth, PO1 3FX, UK

²*Haverford College*

370 Lancaster Ave.

Haverford, PA 19041, USA

³*Oxford Astrophysics*

Denys Wilkinson Building

Keble Road

Oxford, OX1 3RH, UK

⁴*Centre for Astronomy & Particle Theory*

School of Physics & Astronomy

University of Nottingham

Nottingham, NG7 2RD, UK

⁵*European Space Agency*

ESTEC

Keplerlaan 1, NL-2201 AZ, Noordwijk, The Netherlands

⁶*Physics Department*

Lancaster University

Lancaster, LA1 4YB, UK

⁷*Google UK*

Six, Pancras Square

London N1C 4AG

(Received 18th March 2020; Accepted 18th March 2020)

Submitted to AJ

Abstract

Multi-component modelling of galaxies is a valuable tool in the quantitative understanding of galaxy evolution, however it is plagued by issues with convergence, model selection and parameter degeneracies. These issues either limit it to simple models for large samples, or complex models in very small samples (a dilemma we summarize as a choice between “quality or quantity”). This paper presents a novel framework, built inside the Zooniverse citizen science platform, which enables volunteers to help crowdsource the creation of multiple component photometric models of galaxies from SDSS images. We test if this method can help solve the quandry over choosing “quality” or “quantity” for complex galaxy image modelling. We have run the method (including a final algorithmic optimization from the crowd-sourced solution) on a sample of 198 galaxies from the Sloan Digital Sky Survey. We examine the robustness of this new method to variation in population of citizen scientists, as well as compare it to automated fitting pipelines. We demonstrate that it is possible to consistently recover accurate models which show good agreement with, or improve on previous models in the

Corresponding author: Timothy K. Lingard

tklingard@gmail.com

literature. We demonstrate that using citizen science to make selections on number of model parameters to include and their rough optimal values is a promising technique for modeling the images of complex galaxies. We release our catalogue of models to the community.

Keywords: galaxies: spiral — galaxies: photometry

1. INTRODUCTION

Disc galaxies are complex objects, containing many different components, including a disc, disc phenomena (i.e. spiral arms, bars and rings) and central, more spheroidal structures (bulges, bars). Decomposing disc galaxies into their component structures has become an important tool for extragalactic astronomers seeking to understand the formation and evolution of the galaxy population (e.g. [Simard et al. 2002a](#), [Simard et al. 2011](#), [Lackner & Gunn 2012](#), [Kruk et al. 2017](#), [Bamford et al. 2011](#), [Gadotti 2011](#), [Mendez-Abreu et al. 2016](#), [Park et al. 2007](#), [Salo et al. 2015](#)).

These fully quantitative methods allow researchers to obtain structural parameters of galaxy sub-components, which has use in a variety of astrophysical and cosmological research. For example, the stellar mass found in discs and bulges places strong constraints on the galaxy merger tree from Λ CDM N-body simulations ([Hopkins et al. 2010](#)); the strength of a galaxy’s classical bulge is thought to be tied to the strength of a merger event in its past ([Kormendy et al. 2010](#)); different spiral arm formation theories vary in their predictions of spiral morphology ([Dobbs & Baba 2014](#), [Pour-Imani et al. 2016](#), [Hart et al. 2017](#)).

The usefulness of obtaining parametric models of a galaxy has motivated the creation of many image modelling and fitting suites, including GIM2D ([Simard et al. 2002b](#)), GALFIT ([Peng et al. 2002](#)), MEGAMORPH ([Bamford et al. 2011](#)) and PROFIT ([Robotham et al. 2016](#)) to name a few. Using these tools, researchers have built large catalogues of model fits to galaxies. Perhaps most notably [Simard et al. \(2011\)](#) performed two-dimensional, Point-Spread-Function (PSF) convolved, two-component (bulge + disc) decomposition of 1,123,718 galaxies from the Legacy imaging of the Sloan Digital Sky Survey (hereafter SDSS) Data Release 7 ([Abazajian et al. 2009](#)). Other large catalogues of photometric fits exist: [Gadotti \(2011\)](#) made use of parametric multi-band light distribution modelling to model stellar bars in 300 galaxies, [Mendez-Abreu et al. \(2016\)](#) made use of a human-supervised approach to perform multi-component decomposition of 404 galaxies from the CALIFA survey ([Sanchez et al. 2011](#)).

However, despite the usefulness of this technique and the presence of analytic profiles and methods for modelling more complex galaxy sub-components, relatively few studies have attempted to perform large-scale (1000s of galaxies) parametric decomposition of galaxies using more complicated models than that of [Simard et al. \(2011\)](#). Not properly taking into account these “secondary” morphological features (such as a bar, ring and spiral arms) can impact detailed measurements of a galaxy’s bulge ([Gao & Ho 2017](#)). Proper decomposition of secondary morphological features allows investigation into mechanisms behind the secular evolution of galaxies ([Kruk et al. 2018](#), [Gao et al. 2018](#), [Head et al. 2015](#)) and exploration of environmental effects on morphology, such as offset bars ([Kruk et al. 2017](#)).

A prominent issue when performing these detailed decompositions is the tendency for fitting functions to converge on unphysical results when not properly guided or constrained, for instance a Sérsic bulge swapping places with an exponential disc component. It is also the case that often, without near-optimal starting points, detailed model fits will fail to converge at all ([Lange et al. 2016](#)).

Compounding this, uncertainties reported by many software fitting packages (i.e. GALFIT and MEGAMORPH from the above list) are lower estimates on the real uncertainty, due to secondary sources not being modelled, flat-fielding errors and incorrect models ([Peng et al. 2010](#)). Other packages such as GIM2D and PROFIT attempt to fully model posterior distributions and so produce more representative uncertainties, however this comes with a larger computational cost and configuration complexity. These uncertainties are all measures of the likelihood space, and are also only truly valid if the model used is correct.

Another problem which needs to be addressed is whether a component should be present in the model at all. An automated fit will generally attempt to add as many components as possible to produce the closest-matching model. Many studies therefore need to select the most appropriate model by visual inspection of the resulting residuals or recovered parameters. For example, both [Vika et al. \(2014\)](#) and [Kruk et al. \(2018\)](#) inspected the resulting model and residual images for all of their parametric fits (163 and 5,282 respectively) to ensure physical results with the correct components present. The end result of most of these problems is that researchers will have to invest time to individually check many of their fits to ensure they have converged on a physical model. In the era of large sky surveys such as the SDSS ([Abazajian et al. 2009](#)), which in total imaged over 50 million galaxies, the time required to

do this becomes unsustainable and introduces concerns over human error if done by only a single, or small number of individuals.

A demonstrably successful solution to the similar problem of galaxy classification in the era of large surveys, was to find a new source of person-power: [Lintott et al. \(2008\)](#) invited large numbers of people to classify SDSS-images of galaxies over the internet in the Galaxy Zoo project. The resulting classifications (a mean of 38 per galaxy) were then weighted and averaged to create a morphological catalogue of 893,212 galaxies. This hugely successful project, including its subsequent iterations and expansions (i.e. [Willett et al. 2013](#), [Hart et al. 2016](#), [Willett et al. 2017](#), [Simmons et al. 2017](#)), has produced a large catalogue of detailed morphological classifications which are in good agreement with other studies, and have been used in a wide variety of studies of the local galaxy population (see [Masters & the Galaxy Zoo Team 2019](#) for a recent review).

In this paper we explore an analogous solution to that [Lintott et al. \(2008\)](#) brought to galaxy classification for the issues faced by galaxy parametric modelling, inside the ecosystem that Galaxy Zoo set in motion (namely *The Zooniverse*¹). We leverage citizen scientists to pick model components and perform model optimization in an online, web-browser environment². We describe our method in Section 2, including details of the images and ancilliary data from SDSS as well as the strategy used to obtain scientifically useful models from volunteer classifications. We provide consistency checks within our infrastructure and to other methods in Section 3.

Where necessary, we make use of $H_0 = 70 \text{ km s}^{-1} \text{ Mpc}^{-1}$.

2. METHOD

2.1. *The Galaxy Builder Zooniverse project*

Galaxy Builder is a citizen-science project built on the Zooniverse web platform. It asks volunteers to perform detailed photometric modelling of spiral galaxies (potentially including bulge, disc, bar and spiral arm components). A project of this kind, allowing volunteers to interact with and model data, had never been attempted inside the current Zooniverse web platform before, so this project involved designing and implementing a model rendering³ suite inside the existing Zooniverse front-end code-base. As with all citizen science solutions, we had to not only consider the accuracy of the resulting model, but also user experience and engagement in our design decisions.

The closest relative to this project within the Zooniverse ecosystem was the Galaxy Zoo: Mergers project ([Holincheck et al. 2016](#)). This project asked volunteers to help match the morphological properties of an image of merging galaxies to a plethora of restricted three-body simulations, in an attempt to identify the initial conditions that could result in the observed morphology. For part of the project, volunteers downloaded a Java applet, which would run restricted three-body simulations and generate output images. Volunteers could manipulate the model parameters used in the simulation, and vote on simulations which matched a given galaxy merger image or shared important tidal features. A new batch of simulations could then be run and an optimal solution converged on.

In many ways, this iterative workflow was very similar to that used in *Galaxy Builder*: volunteers were asked to manipulate the parameters of a complex astrophysical model in order to identify the most likely solution, in a problem space that traditional computational modelling struggles to solve. However, *Galaxy Builder* operates purely inside a web page and does not make use of secondary citizen science projects for model selection (such as the Galaxy Zoo: Mergers’ *merger wars* sub-project), instead using unsupervised clustering and computational optimization to identify final models.

2.1.1. *Project Timeline and Development*

The *Galaxy Builder* project was built inside the Zooniverse’s ([Simpson et al. 2014](#)) PANOPTES-FRONT-END⁴ code-base, using Facebook’s REACT.JS⁵ framework, as well as WebGL⁶ to enable low-latency photometric galaxy model rendering. *Galaxy Builder* entered a Zooniverse beta in late November 2017 and after some user experience improvements and code refactoring, the project was launched as an official Zooniverse project on the 24th of April 2018.

A major challenge during development of the project was finding the right balance between keeping a simple and intuitive interface and workflow while also allowing the freedom and versatility to properly model galaxies. It was

¹ <https://www.zooniverse.org>

² <https://www.zooniverse.org/projects/tingard/galaxy-builder>

³ We use the term rendering in a similar manner to that used for computer graphics: to calculate an image from a model or set of rules.

⁴ <http://github.com/zooniverse/Panoptes-Front-End>

⁵ <https://reactjs.org/>

⁶ <https://www.khronos.org/webgl/>

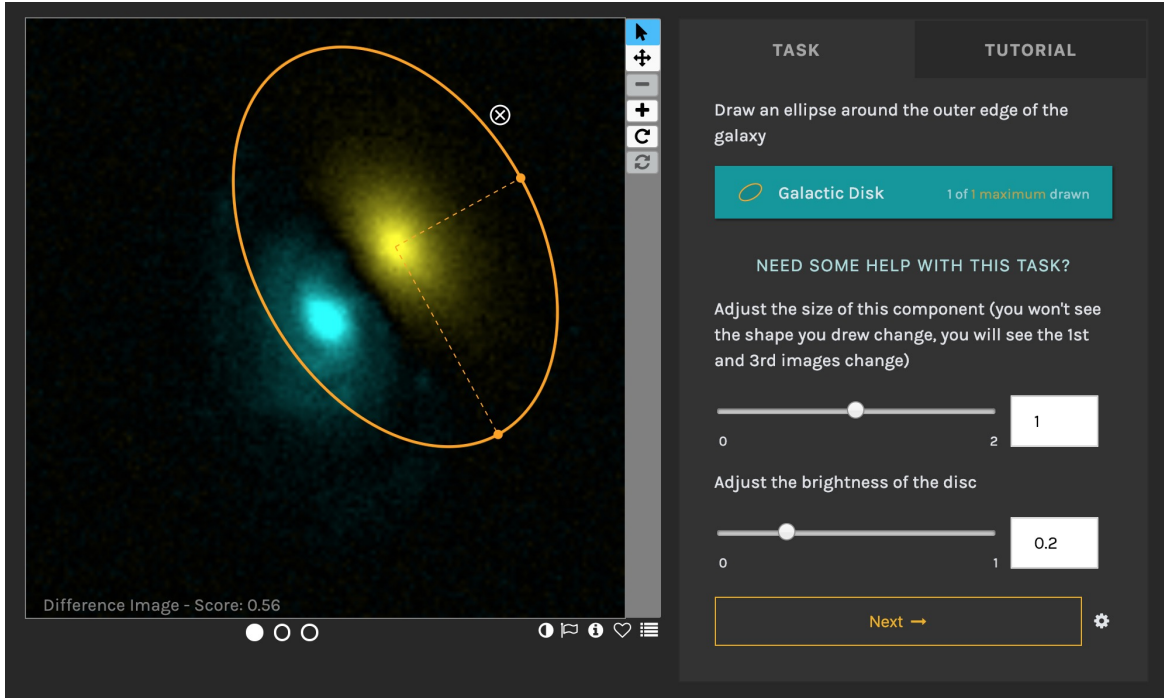


Figure 1. The *Galaxy Builder* interface. The residual image is being shown, and the volunteer is on the “Disc” task. The drawn disc component (yellow) is offset from the galaxy image (blue) to demonstrate the positive and negative residuals. Where the image equals the model the residual is black. The dots below the residual image allow the user to switch images. The icons to the right allow panning and zooming of the image (rotation was not functional for this project). The icons to the bottom right of the image allow colour inversion of the galaxy cutout, flagging of the image as inappropriate, inspection of galaxy metadata (i.e. sky position, link to SDSS SkyServer), ability to save the image as a favourite and to add to a Zooniverse “collection”. The Score shown in the bottom left of the image is calculated using Equation 1 and is a rough goodness-of-fit measure.

also a significant challenge to develop a compelling and simple tutorial for what is one of the most complex projects attempted on the Zooniverse platform. Feedback from expert users was essential to this process as part of the the typical beta trial process for Zooniverse projects⁷.

2.1.2. The project interface

The *Galaxy Builder* project prompts volunteers to work through the step-by-step creation of a photometric model of a galaxy (described in detail in Section 2.4). The interface presents a volunteer with three views, which they can switch between at any time: a *r*-band cutout image of a spiral galaxy (see Section 2.2), the galaxy model they have created so far, and the residual between their model and image (shown in blue and yellow). A screenshot of the interface can be seen in Figure 1, where a residual image is shown.

The workflow is designed so that volunteers slowly subtract increasing amounts of light from the galaxy, as can be seen in Figure 2. A tutorial is available which contains a step-by-step guide to completing a classification. At each step volunteers are asked to first draw a simple isophote, and then make use of a series of sliders to adjust the parameters of the model component (see Section 2.4 for more information).

Volunteers are also guided by a “score”, which is tied to the residuals and chosen to increase from zero to some arbitrary value depending on the galaxy; a less noisy and more easily modelled galaxy will have a higher maximum score. To map a residual image to a final score shown to volunteers we used

$$S = 100 \exp \left(\frac{-A}{N} \sum_{i=0}^N \frac{\operatorname{arcsinh}^2 (|y_i - M_i| / 0.6)}{\operatorname{arcsinh} 0.6} \right), \quad (1)$$

⁷ <https://help.zooniverse.org/best-practices/>

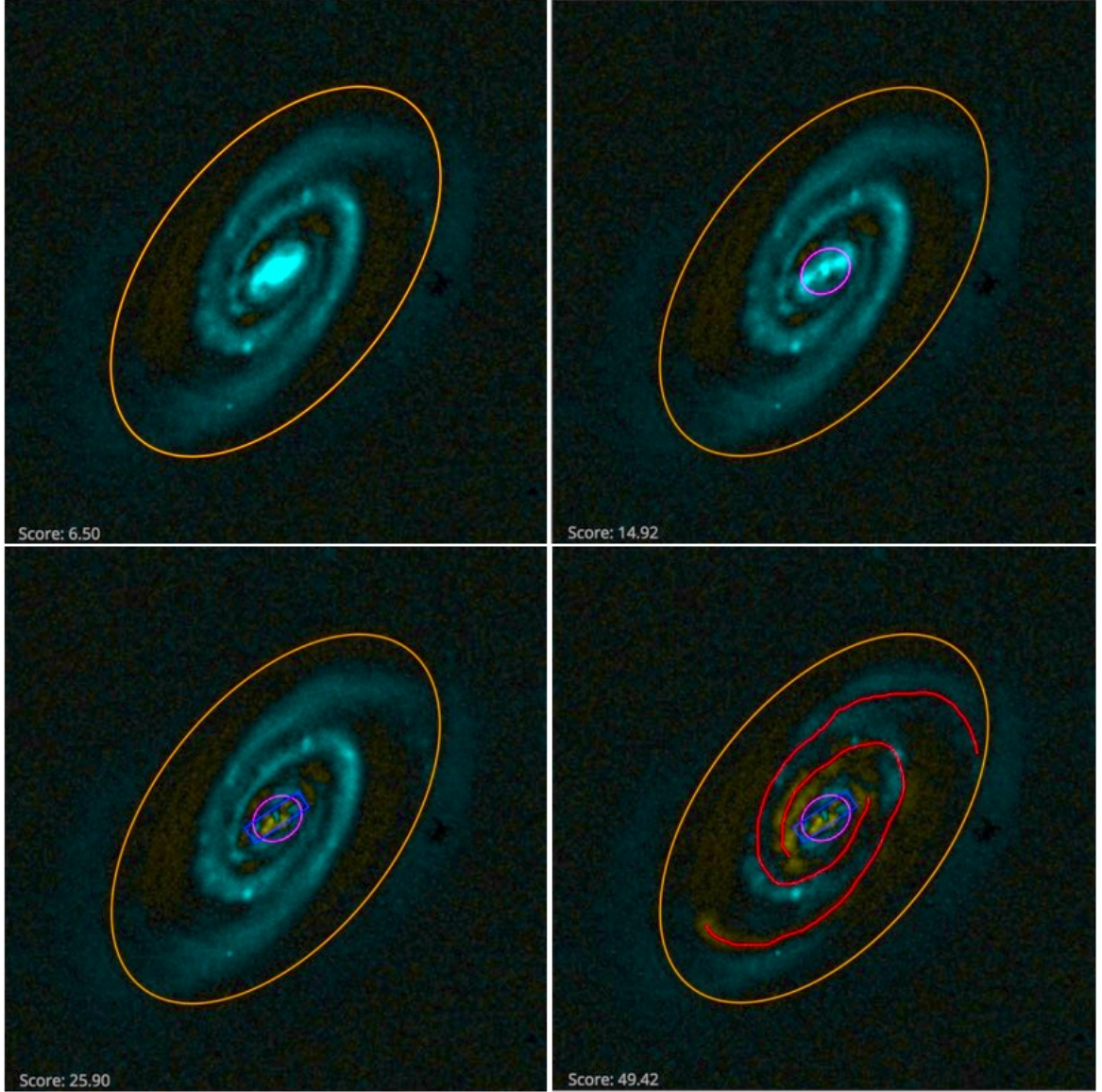


Figure 2. Figure demonstrating the desired result of each step of the modelling process, as seen from the residual image provided to volunteers. The top left panel shows the galaxy after only a disc component has been added: the top right contains a disc and a bulge; the bottom left has a disc, bulge and bar; the bottom right is the finished model with a disc, bulge, bar and spiral arms. The images shown is SDSS J104238.12+235706.8. This brightness and contrast of this image have been edited to improve visibility in print.

where N is the total number of pixels, y is the cutout of the galaxy, normalized to a maximum value of 1 ($y = \text{cutout}/\max(\text{cutout})$), M is the model calculated by volunteers and $A = 300$ is an arbitrary choice of scaling chosen based on a handful of test galaxies.

This score has the advantage of being easy (and fast) to generate from the residual image shown to volunteers (which was Arcsinh-scaled in a manner described by [Lupton et al. 2004](#)), however it is quite sensitive to small deviations of the model from the galaxy.

2.2. Sample Selection: Images and Ancillary Data

Galaxy Builder finds a niche with complex, multi-component galaxies. As such, the sample should be selected to have these features. The original sample proposed for the *Galaxy Builder* project aimed to mirror the *stellar mass-complete*

Table 1. The selection criteria used in Hart et al. (2017) to create the *stellar mass-complete sample* of 6222 spiral galaxies.

Description	Value
Face-on spiral morphological selection.	$\text{GZ2 } p_{\text{features}} \cdot p_{\text{not edge on}} \cdot p_{\text{spiral}} \geq 0.5$
Redshift limits.	$0.02 < z < 0.055$
Face-on galaxy selection using g-band axial ratio.	$(b/a)_g > 0.4$
Volume correction.	$9.45 < \log(M_*/M_\odot) \leq 11.05$
Computation of stellar mass completeness limits using the method of Pozzetti et al. (2009) and limits calculated by Hart et al. (2017).	$2.07 \log(z) + 12.64 < \log(M_*/M_\odot) < 2.45 \log(z) + 14.05$

sample in Hart et al. (2017). This was a sample of face-on spiral galaxies, with and without bars, complete in stellar mass.

The morphological information required to select spiral galaxies came from the public data release of Galaxy Zoo 2 (Willett et al. 2013, hereafter GZ2). Each response to a GZ2 morphology question is allocated a p value ranging from 0 to 1, where 0 indicates no volunteers responded positively to that question and 1 indicates all volunteers who classified that galaxy responded positively (i.e. $p_{\text{bar}} = 0.5$ would indicate 50% of volunteers said a bar was present in a galaxy). Photometric measurements used for selection came from the NASA-Sloan Atlas (Blanton et al. 2011, hereafter NSA). The *stellar mass complete sample* is constructed using the set of criteria detailed in Table 1.

The *stellar mass-complete sample* was split into smaller sub-samples, each containing 100 galaxies. In an iterative process, each sub-sample was chosen to contain the 60 lowest redshift unclassified galaxies, and 40 random unclassified galaxies. This was done to account for the unknown rate at which volunteers would provide classifications. In the first two sets of 100 galaxies, 1% of galaxies (i.e. 2 images) failed to run through the image preparation process, due to an error when attempting to montage multiple frames. The root cause of this error is unknown, but it leaves a sample of 198 galaxies with images that are considered in this paper.

2.2.1. Image and modelling metadata extraction

The galaxy data shown to volunteers in the *Galaxy Builder* project came in two forms: A gray-scale image cutout of the galaxy and a JSON file containing rendering information for the web-interface.

Both forms of data were obtained using a similar process:

- A montage of multiple r-band corrected frames from the SDSS DR13 (Albareti et al. 2017) data release was created. To combine multiple FITS images, we made use of Astropy (Astropy Collaboration et al. 2018), and the MONTAGE (Jacob et al. 2010) software package.
- This montage was cropped to four times the Petrosian radius of the galaxy.
- The SExtractor software (Bertin & Arnouts 1996) was used to identify regions containing secondary sources (foreground stars, other galaxies) and generate a mask.
- A PSF was obtained from the relevant Sloan r-band `psField` file, extracted at the central position of the galaxy (Stoughton et al. 2002).
- The JSON file was written containing the cut-out data and the 2D boolean mask obtained from the source extraction process. This file also contained other metadata needed for the rendering process (PSF, the size of the PSF array, and the width and height of the image).
- Another JSON file containing simply the information used to render the volunteer’s model (image size and PSF) was created.
- An arcsinh-stretch was applied to the masked cutout (as described by Lupton et al. 2004). It was then saved as a grey-scale image.

The decision to use r-band images in our subject set was due to its higher signal-to-noise than other bands.

Once a sub-sample had been created, the Zooniverse’s PANOPTES-PYTHON-CLIENT⁸ was used to upload them as a subject-set to the Zooniverse.

Upon later consideration (after subjects had been uploaded to the Zooniverse), it was determined that the reprojection performed by MONTAGE has a smoothing effect on the data, and thus does not conserve errors. This motivated the calculation of a separate stacked image, sigma image and corresponding pixel mask, using the same r-band corrected frames present in the montage, as described in Appendix A. These images were not shown to volunteers but were used for model fitting and comparison.

2.3. Choice of Retirement limit

Initially 10 classifications were collected per galaxy, however preliminary analysis indicated this number of independent answers was insufficient to create reliable and reproducible aggregate classifications. For this reason, a hand-picked sample of 56 galaxies was then re-activated with a retirement limit of 30 classifications per galaxy. This sample was chosen by eye to be a relatively diverse set of galaxies, most with prominent spiral features including grand-design and flocculent arms. Its purpose was to allow the development of the aggregation methodology.

Once this hand-picked sample was completed, and it had been determined that 30 classifications per galaxy was sufficient, the remaining galaxies from the initial two sub-samples were re-activated, as well as a repeat of the first sub-sample (hereafter the *validation subset*) to measure volunteer consistency. This paper focuses on these 198 galaxies (presented in *Galaxy Builder* as 296 separate images) in order to explain the method used, and test the reliability of the models obtained.

We also created 9 synthetic images of galaxies, containing various combinations of components available to volunteers and a spread of possible parameters. These synthetic galaxies were based off of a set of target galaxies from galaxy builder, including the use of the galaxies’ metadata for the addition of realistic noise and pixel masks. This set of synthetic images was used to calibrate our aggregation and fitting methodology and thus is referred to as the *calibration subset*.

2.4. The Galaxy Model

The model chosen was largely based on components described in Peng et al. (2002). The model components consisted of:

1. An exponential, elliptical disc.
2. An elliptical Sérsic bulge, with n chosen by volunteers and allowed to vary from 0.5 to 5.
3. A Sérsic bar with a “boxiness” modifier (as described in Peng et al. 2002).
4. Any number of freehand poly-line spiral arms, as described below.

Each spiral arm is modelled using a poly-line drawn by the volunteer. The brightness of a spiral arm at any point is given by the value of a Gaussian centred at the nearest point on any drawn poly-line, with volunteers able to choose the Gaussian width and peak brightness using sliders. Radial falloff was added by multiplying by the value of the previously added exponential disc, though volunteers could change the half-light radius of this falloff disc.

The modelling code ignores masked regions identified as secondary sources by SExtractor. It over-samples the bulge, disc and bar components by a factor of five and performs PSF convolution using a PSF obtained from the relevant Sloan r-band `psField` file, extracted at the central position of the galaxy (Stoughton et al. 2002).

2.5. Reprojection of Classifications into original SDSS Frame Coordinates

In order to properly account for errors and as part of the data reduction process, we transform all classifications recieved for a galaxy from the coordinate space of the MONTAGE-created cutouts shown to volunteers to the WCS of the original frames, allowing the use of the accurate sigma images discussed in Section 2.2.1.

⁸ <https://github.com/zooniverse/panoptes-python-client>

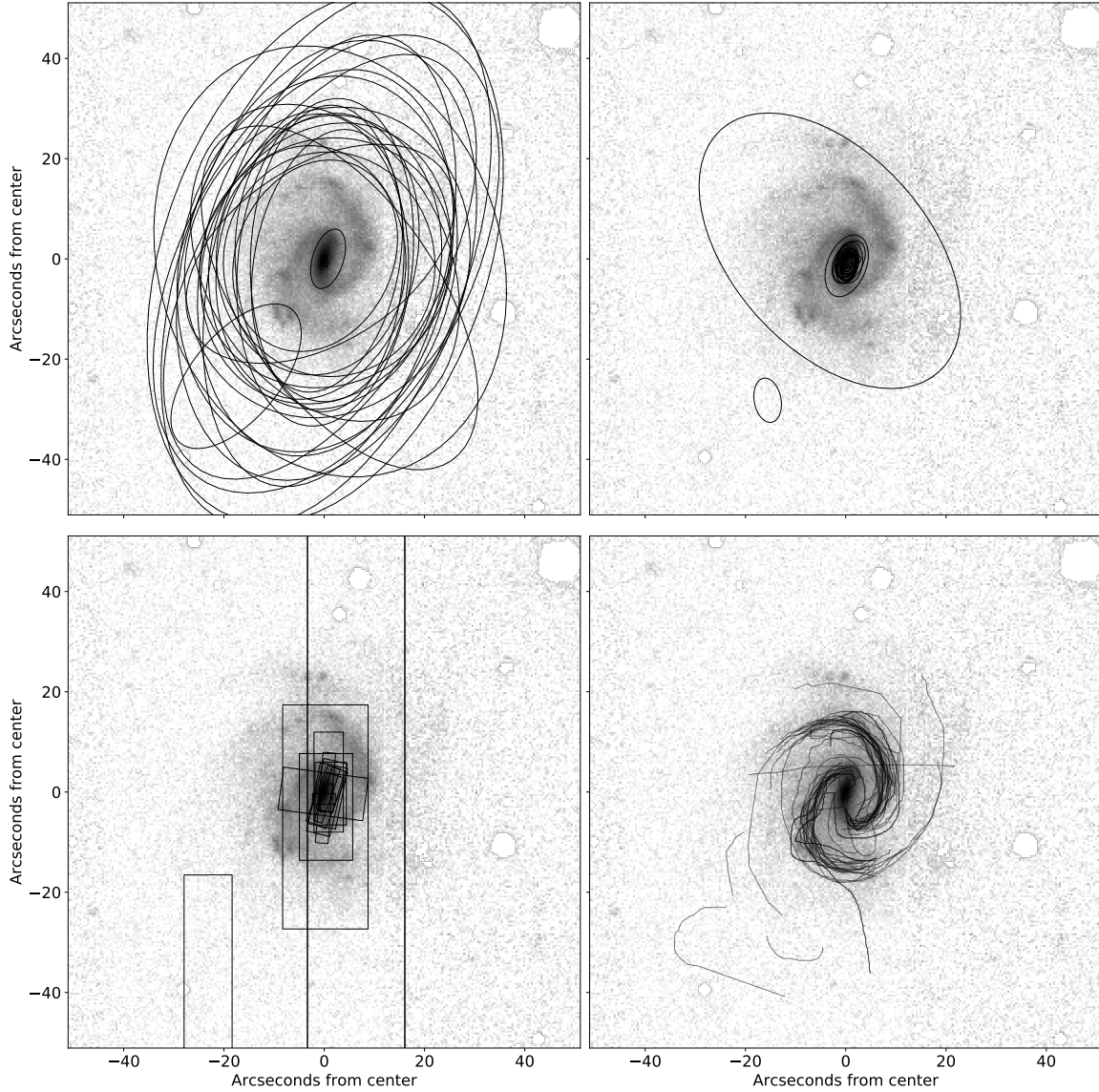


Figure 3. Components drawn by volunteers for UGC 4721. The top left panel shows drawn discs, top right shows drawn bulges, bottom left shows drawn bars and bottom right shows drawn spiral arms. Discs, bulges and bars are displayed at twice their effective radii.

2.6. Classification Aggregation Methodology

In this Section, we will use the galaxy UGC 4721, a two-armed barred spiral galaxy at $z = 0.02086$ classified by [de Vaucouleurs et al. \(1991\)](#) as SBcd, to illustrate the data reduction and aggregation methodology. For UGC 4721 we received 32 classifications, containing 28 discs, 24 bulges, 17 bars and 47 drawn spiral arm poly-lines. These annotations can be seen in Figure 3, overlaid on the greyscale r-band image of the galaxy.

2.6.1. Aggregation of Volunteer Models

Aggregate model calculation was done on a component-by-component basis, rather than per classification, i.e. clustering of discs was performed independently to that of bulges, bars and spirals. We did not take into account any slider values, only the shape drawn by the volunteers. Disk classifications were doubled in effective radius to account for an observed tendency of volunteers to draw a smaller disk than needed. Clustering was performed using the Jac-

card distance measure (also known as the intersect-over-union distance, or IOU distance), which is a simple metric determining the relative shared area of two sets:

$$d_J(A, B) = 1 - \frac{|A \cap B|}{|A \cup B|}. \quad (2)$$

The algorithm chosen to perform clustering was the density-based spatial clustering of applications with noise (DBSCAN, [Boonchoo et al. 2018](#)) algorithm, due to its robustness and speed. We made use of Scikit-learn ([Pedregosa et al. 2011](#)) to implement the algorithm. In DBSCAN the core of a cluster is defined as a group of at least `min_points` that are all within a distance `eps` of each other. Additionally, any points within a distance `eps` of a cluster’s core are also associated with the cluster. The values of `eps` and `min_points` for the disk and bulge were chosen by visually inspecting the resulting clustering results and ensuring that a disc was obtained for all galaxies, and a bulge for most. The value of `eps` used to cluster bars was tuned such that the aggregate model best agreed with GZ2 p_{bar} ($p_{\text{bar}} < 0.2$ implying no bar and $p_{\text{bar}} > 0.5$ implying a definite bar). The values chosen for `eps` were 0.3, 0.4, 0.478 for the disc, bulge and bar; `min_points` was set to 4 for all three of these components.

Prior to clustering, models were altered such that component parameters were within the limits shown in Table 2 (deemed to be the physically acceptable bounds for such a component).

For shapes clustered in this way, we define the aggregate component to be the shape which minimises the sum of Jaccard distances to each of the shapes in the cluster. For our example galaxy, UGC 4721, clustered and aggregate components can be seen in Figure 4.

To cluster drawn spiral arms, we define a custom separation measure to represent how far away one poly-line is from another. This measure was chosen to be the mean of the squared distances from each vertex in a poly-line to the nearest point (vertex or edge) of another poly-line, added to the mean of the squared distances from the second poly-line to the first. We make use of this separation measure inside the DBSCAN algorithm to cluster these drawn lines, after removing any self-intersecting drawn arms (as this was deemed an easy method to filter out “bad” classifications). Values of 0.001 and 4 were used for the `eps` and `min_samples` hyper-parameters respectively.

Once spiral classifications on a galaxy have been clustered into the physical arms they represent, the points are deprojected using the axis ratio and position angle of the aggregated disc. The deprojection method assumes a thin disc and stretches the elliptical minor axis to match the major axis.

Deprojected points within each drawn poly-line are converted to polar coordinates and unwound to allow model fitting. These unwound points are then cleaned using the Local-outlier-factor algorithm (LOF, [Breunig et al. 2000](#)). For each drawn poly-line in the cluster, the LOF algorithm was trained on all points not in that arm, and then used to predict whether each point in the arm should be considered an outlier. In this way we clean our data while respecting its grouped nature. The points removed as outliers for the example galaxy are shown in the bottom right panel of Figure 4.

For each arm cluster in each galaxy, a logarithmic spiral model was fitted using Bayesian Ridge Regression, performed using the Scikit-learn python package. Hyperpriors on the noise parameter were chosen by fitting a truncated gamma distribution ([Zaninetti 2014](#)) to the spiral width slider values returned by volunteers (ignoring sliders left at the default or moved to the extremes of allowed values). Any logarithmic spirals within a distance of 0.0005 (given by the clustering metric) were deemed to be from the same arm and thus their classifications were merged and a log-spiral recalculated.

To obtain a single value for the pitch angle of a galaxy, we take the length-weighted average pitch angle of all arms detected in the galaxy (as used by [Davis & Hayes 2014](#)).

The galaxy model for UGC 4721 obtained through aggregation can be seen in the bottom left panel of Figure 5.

2.7. Error Estimation of Aggregate models

As all components in a cluster can be viewed as volunteers’ attempts at modelling the true underlying component, the sample variance of the parameters of these shapes can be used as a measure of confidence in the parameters present in the aggregate result. These are highly sensitive to clustering hyperparameters, and are only valid for a component’s position, size and shape. Figure 4 illustrates the variance in clustered shapes for our example galaxy (UGC 4721); we see a large variation in the clustered discs, and much closer agreement on bulge and bar size and shape.

2.8. Model Fitting

As mentioned above, the need for a numerical fit to fine-tune parameters of *Galaxy Builder* models was anticipated. This fitting was performed using the L-BFGS-b algorithm ([Byrd et al. 1995](#)), implemented in SCIPY ([Jones et al.](#)

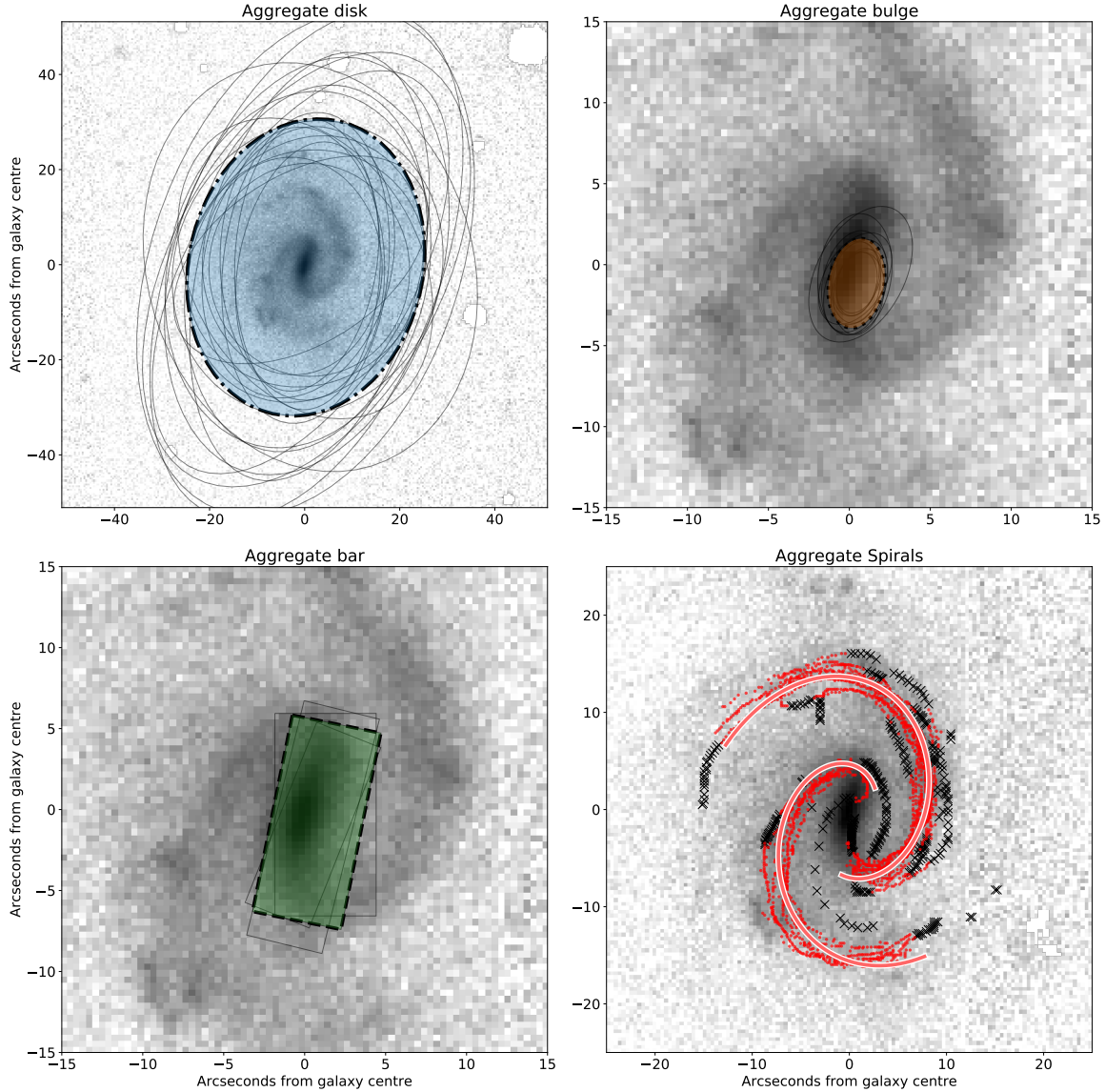


Figure 4. Calculated aggregate components for UGC 4721. The aggregate disk is shown using a dot-dashed line and blue fill in the upper left panel, the aggregate bulge with a dotted line and orange fill in the upper right panel, the aggregate bar using a dashed line and green fill in the lower left panel and the aggregate spiral arms are plotted as red lines in the lower right panel. Sérsic components are displayed at twice their effective radii. Black crosses in the lower right panel indicate spiral arm points that were identified as outliers and removed during cleaning.

2001). We minimize a custom likelihood function that assumes gaussian error on pixel values and incorporates the priors on parameters we obtain from clustering. The full fitting model and likelihood is detailed in Appendix B. We use the same model as used by volunteers in the online interface (with altered limits), with spiral arms restricted to being logarithmic spirals relative to the disc, and without the ability to change the relative falloff of spiral arms.

The model rendering and fitting code was written up using Google’s JAX package (Bradbury et al. 2018), which allows GPU-optimization and automatic gradient calculation, enabling quick and accurate calculation of the jacobian matrix needed for the L-BFGS-b minimization algorithm.

Before fitting for all free parameters, we fit only for the brightnesses of components. The result of the fit, including the final photometric model for UGC 4721, can be seen in 5. The secondary components have been accounted for well, and the model has a sensible reduced chi-squared value of 1.176, where we have approximated degrees of freedom as the number of unmasked pixels present in the galaxy image (similar to GALFIT).

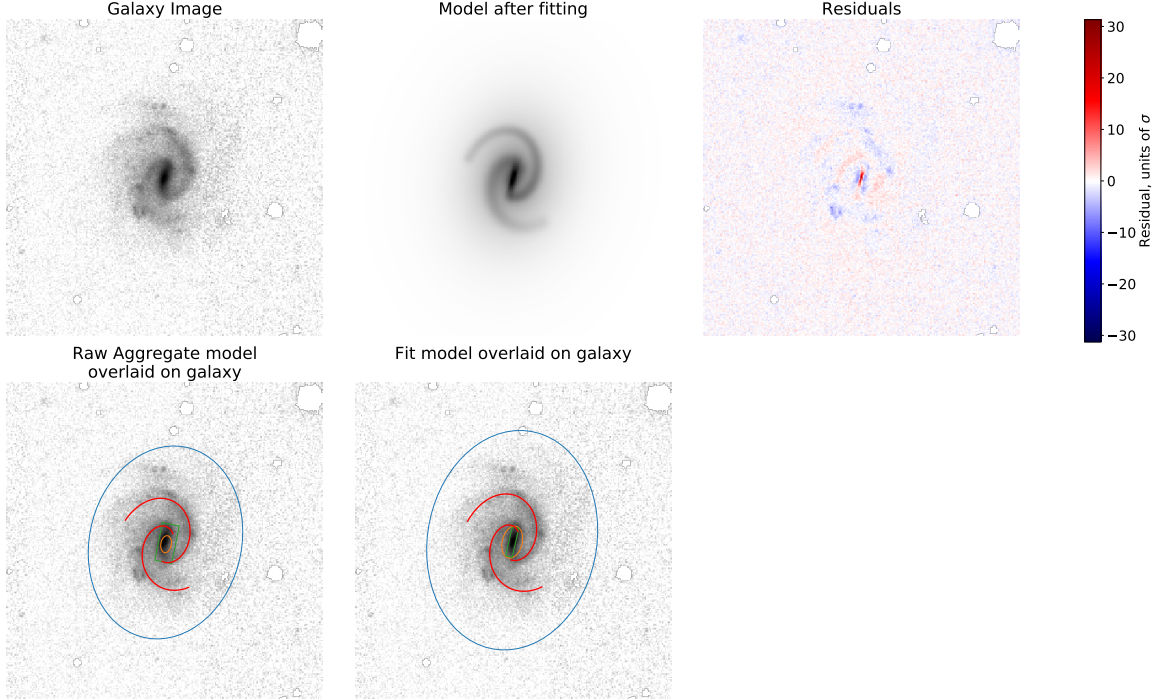


Figure 5. Effect of fitting on the fit results. The top left panel shows an Arcsinh-scaled image of the galaxy being fit (UGC 4721), the top middle shows the final model obtained (with the same limits and scaling as the galaxy image) and the top right shows the difference between the two images, in units of pixel uncertainty. The bottom panels show a simple representation of the model before and after tuning, overlaid on the galaxy image from the top-left panel.

As we do not perform a full Bayesian minimization, we make use of the errors described in Section 2.7 as our parameter uncertainties, as we feel a Hessian-based approach would likely fall foul of the issues described in the introduction and thus be a under-estimate, this does mean we do not have uncertainties for some parameters.

3. RESULTS

In this Section we explore the consistency with which volunteers modelled galaxies, the accuracy of the aggregate models, and compare the aggregate and fitted models to comparable results in the literature.

3.1. The Calibration Set

The recovered models for the nine synthetic galaxy images created for the *calibration subset* show that volunteers make systematic use of bulges, even when only a bar component is needed, resulting in two Type 1 errors for bulge presence in the aggregate model. It also highlighted the limitation of the Jaccard metric for highly elliptical components (i.e. bars), as even a small change in rotation results in a large change in the metric. The result of this is one Type 2 error of bar presence in the aggregate. We successfully recover all spiral arms present, and do not receive any false positives. The pitch angles obtained through aggregation vary by up to 9° from the true values, with fitting improving this error slightly.

Fitting also highlighted the difficulty in recovering structural parameters for which we did not obtain a starting point through clustering (Sérsic index and bar boxyness). These parameters are crucial for measurements of bulge fraction, but difficult to identify using gradient descent (Lackner & Gunn 2012). Reduced Chi-squared values for the fits range from 1.000 to 1.331.

As these galaxies were used to fine-tune clustering and fitting hyperparameters, our ability to recover morphology accurately is essential validation for our ability to recover good photometric models of galaxies. These results highlight the importance of good priors to obtain accurate fits of complex photometric models.

3.2. Examination of Volunteer consistency

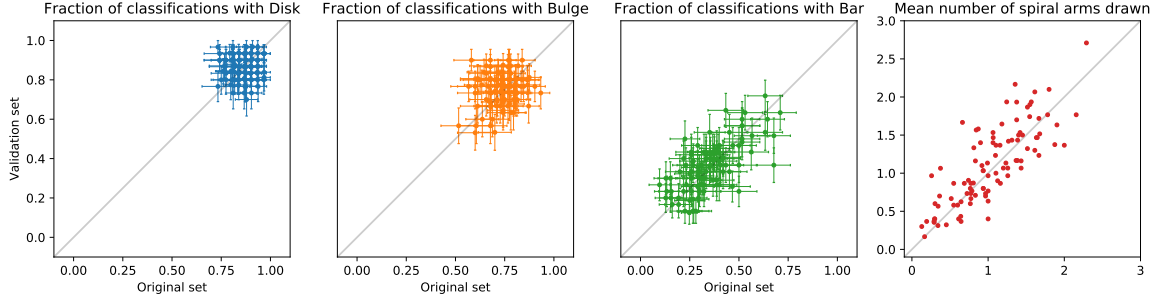


Figure 6. Comparison of frequency of use of component in volunteer models between the original and validation sets of classifications. Errors shown on the disc, bulge and bar arise from Binomial error estimation.

We aggregate two independent models for a set of 98 galaxies based on “original” or repeat (“validation”) classifications, obtained with the same retirement limit (see Section 2.3 for more on this selection).

One of the simplest choices the volunteers have is whether to include a model component or not. Figure 6 illustrates the consistency with which volunteers made use of a component in their model for a galaxy. We see that volunteer classification is very consistent, with scatter as predicted by the Binomial uncertainty on the mean. Volunteers almost always make use of a disc and bulge (as seen in the *calibration subset*), and even proportions agree on the presence of a bar and the number of spiral arms. Many volunteers used a very elliptical bulge and the ends of spiral arms to model light that could be seen classified as a bar. The validation model is identical to the original model for less than 40% of galaxies (often due to a missing bar component or single spiral arm), suggesting further work is needed to ensure consistency in aggregation.

After selecting a component, the volunteer sets its shape and size. Fewer bars being drawn by volunteers makes clustering more difficult and more uncertain; for a strongly barred galaxy with 30 classifications we receive only 15 or so drawn bars. The variation in axial ratios and effective radii for the aggregate discs, bulges and bars are shown in Figure 7. The aggregate discs and bulges are consistent within errors, while bars show more scatter, potentially due to reasons discussed above.

3.3. Comparison to results in the literature

After having obtained aggregated models for our galaxies, we examine how our models compare to other results in the literature. There exists no published comparison sample with four-component fits, instead we make comparisons for individual or subsets of model components.

3.3.1. Comparison to Galaxy Zoo morphology

The simplest comparison we can make to external results is to examine whether our models respect the existing morphological classifications present in the literature. We make use of Galaxy Zoo 2 (GZ2, Willett et al. 2013) results, including the redshift debiasing described in Hart et al. (2016) and spiral properties calculated in Hart et al. (2016).

When comparing the probability of a volunteer’s classification containing a bar component against a galaxy being classed as strongly-barred or as having no bar (as defined in Masters et al. 2010), we see a significant difference: ignoring Binomial uncertainty, classifications of strongly-barred galaxies ($p_{\text{bar}} > 0.5$) had a 0.47 ± 0.15 chance of containing a bar, vs 0.29 ± 0.11 for galaxies classed as having no bar ($p_{\text{bar}} < 0.2$). The Pearson correlation between GZ2’s p_{bar} and the bar likelihood in *Galaxy Builder* is 0.56, implying a significant correlation. We do not compare to the morphology of the aggregate model as we tuned the bar clustering hyperparameters using GZ2 morphologies.

We also compare the number of spiral arms aggregated by *Galaxy Builder* with the responses to the GZ2 “number of arms” question (of which the possible responses were one, two, three, four, more than four or “Can’t tell”). We attempt to account for the spread in volunteer answers to this question by binning responses, rather than using the mean or modal response. The results of this comparison can be seen in Figure 8. The area of each circle can be seen as the level of agreement between *Galaxy Builder* aggregate models and GZ2 classifiers, it is defined as

$$A_{i,j} \propto \sum_k^{N_g} \frac{1}{M_k} \sum_m^{M_k} \begin{cases} 1, & \text{if } n_k = i \text{ and } C_{k,m} = j \\ 0, & \text{otherwise} \end{cases}, \quad (3)$$

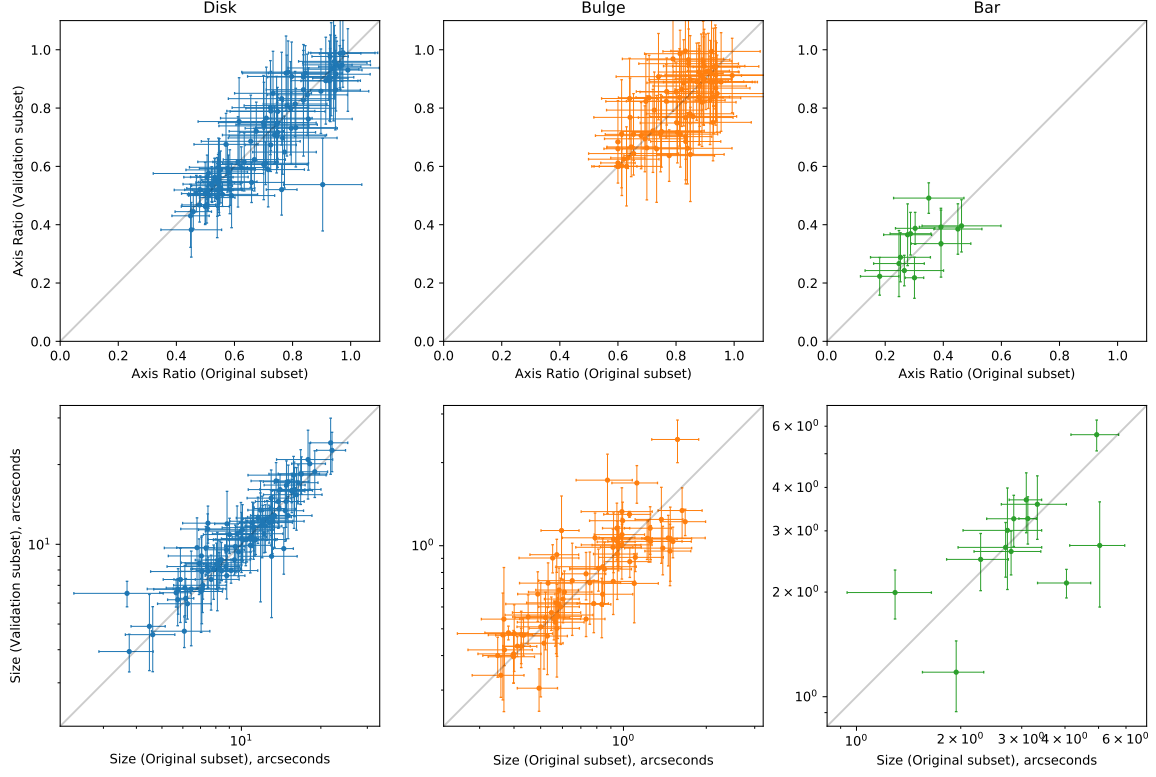


Figure 7. Comparison of component shape in aggregate models between the original and validation sets. Errors are obtained through the sample variance of clustered components, as detailed in Section 2.7.

where n_k is the number of aggregate arms for galaxy k (out of N_g galaxies), $C_{k,m}$ is the m -th answer for galaxy k (out of M_k answers).

The circle with the largest area for each possible GZ2 response is highlighted, and agrees with the number of spiral arms aggregated here for $m = 1, 2, 3, 4$. No aggregate model contained more than four spiral arms, and when galaxies have an uncertain number of spiral arms (the “Can’t tell” GZ2 response) we mostly do not aggregate any spiral arms.

It is not uncommon in *Galaxy Builder* for one spiral arm to have been broken into two smaller segments. We also occasionally identify two distinct clusters that represent the same physical arm. These two reasons account for a majority of cases where GZ2 classifications suggest a galaxy has two spiral arms and we have clustered a larger number. Improved project user experience would be crucial in correcting these errors.

3.3.2. Comparison to One-component fit - axis ratio

We compare the axis ratios of the discs of *Galaxy Builder* aggregate models (without fitting) to the axis ratio of a 2D Sérsic fit to the r-band SDSS image of each galaxy (as provided in the NSA catalog, Blanton et al. 2011). For the untuned models there is an error of ~ 0.1 , consistent with our expected errors (derived in Section 2.7). There is a clustering of outlying values around $b/a = 0.5$ which is almost certainly due to the drawing tool ellipse having a default axis ratio of 0.5. Where this default is a “good enough” fit we hypothesise that volunteers are less likely to modify it, while if it needs to move a long way they find a more refined value.

Volunteers not adjusting components from their default values was a consistent issue with volunteer models (36% of all disc components drawn by volunteers were left at the default axis ratio, and over half of all bars were left with their default rotation, though many of these would have been excluded during clustering). Future projects should carefully consider their interface design to minimize this bias. Fitting aggregate models successfully removes this bias though the overall scatter does not change significantly.

3.3.3. Comparison to Disc-Bulge models

A strong motivation for performing multi-component modelling is the desire to measure the fraction of a galaxy’s light being emitted by its central components (such as bulge fraction, defined as the ratio of bulge luminosity to total

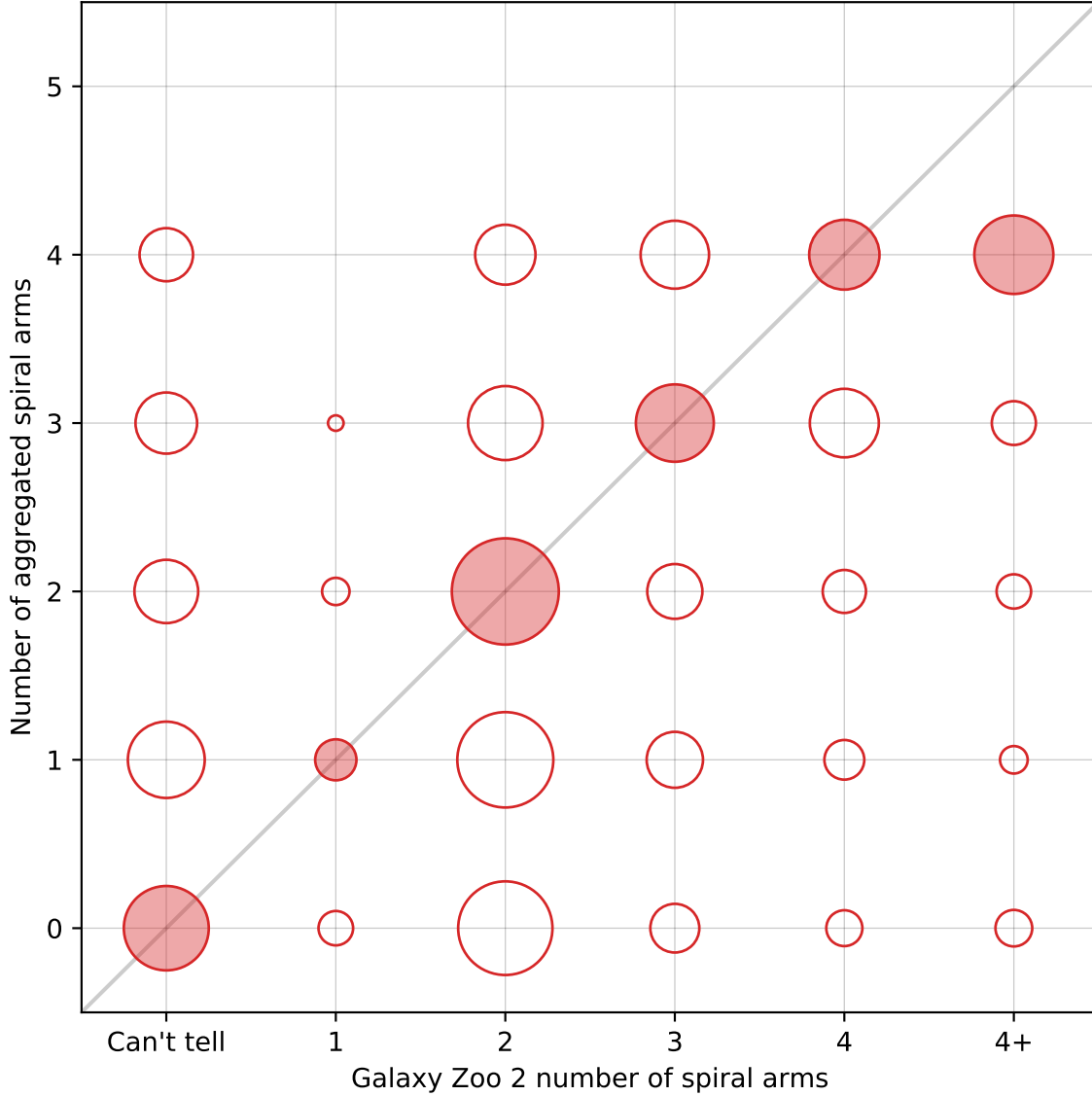


Figure 8. Density plot of GZ2 vote counts for spiral arm number vs the number of spiral arms obtained through aggregation. The area of each circle can be seen as the level of agreement between *Galaxy Builder* aggregate models and GZ2 classifiers, and is defined by Equation 3. The circle with the largest area for each possible GZ2 response is highlighted by shading.

luminosity). [Gao & Ho \(2017\)](#) demonstrate that modelling secondary central components is essential for recovering an accurate measure of bulge fraction. The difficulty of measuring bulge fraction is further compounded by the complex degeneracies present in even two-component fits, meaning that many gradient-descent based solvers often fail to find the globally optimum solution ([Robotham et al. 2016](#)), especially when bulge Sérsic index is a free parameter.

One of the largest catalogs of 2D multi-component fits is [Simard et al. \(2011\)](#), which performed simultaneous, two-bandpass decompositions of 1,123,718 galaxies in the Legacy area of the SDSS DR7 using GIM2D. Three variations of models were fitted: a pure Sérsic model, an Exponential disc and de-Vaucouleurs bulge model (hereafter exp+deV), and an Exponential disc and a Sérsic bulge model (exp+S). Fitting was performed using the Metropolis algorithm, which is resilient to local minima and therefore suitable for the complex likelihood space of galaxy photometric modelling. [Lackner & Gunn \(2012\)](#) similarly fitted two models to SDSS main-sample galaxies: an exponential disc and exponential bulge (exp+exp), and an exponential disc and de Vaucouleurs bulge. They used a Levenberg-Marquadt gradient descent algorithm, with initial parameters taken from previous SDSS analysis.

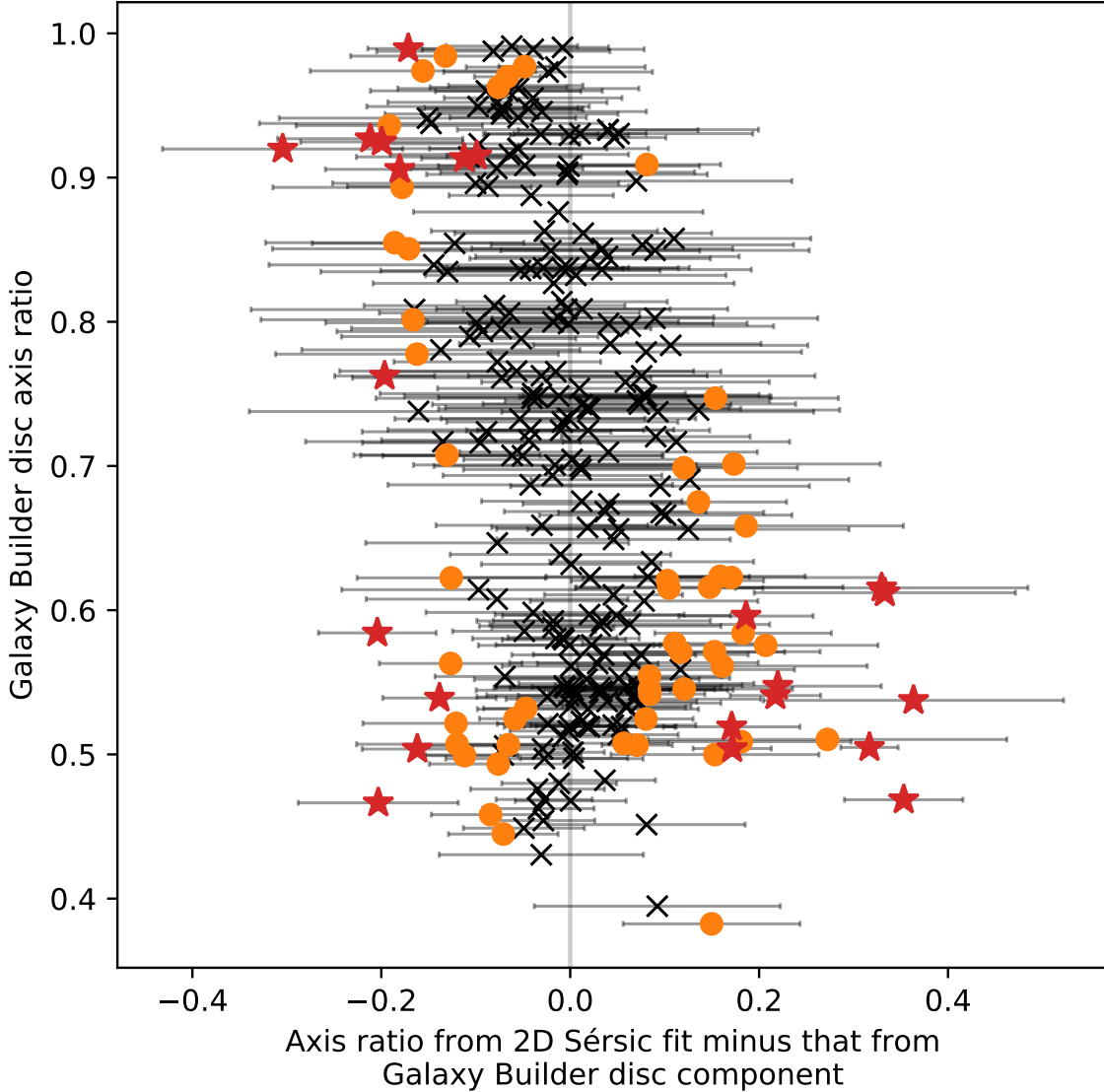


Figure 9. Difference between the axis ratios of the aggregated disc component (before fitting) to the results of an r-band Sérsic profile fit. Points between one- and two-sigma are highlighted as orange squares, points outside two-sigma are shown as red stars.

We compare our central component fraction to bulge fraction from [Simard et al. \(2011\)](#) where their analysis indicated genuine bulge+disc systems ($P_{pS} \leq 0.32$). We compare to [Lackner & Gunn \(2012\)](#) bulge fractions only when their model selection criteria determined that model was the best-fit model. We see a significant scatter, but a strong correlation (Figure 10). We note that the relationship to exp+deV models appears to be less than 1:1, while the relationship to exp+exp models is greater than 1:1, highlighting the dependance of bulge fraction on Sérsic index. The amount of scatter (and lack of consistent 1:1 relationships) between bulge fractions of the two-component models is comparable to the scatter we see to our more complex one.

3.3.4. Comparison to Disc-Bulge-Bar models

[Kruk et al. \(2018\)](#) performed multi-component, multi-band decompositions of a selection of SDSS galaxies, 12 of which were also classified in *Galaxy Builder*. Figure 11 compares the axis ratios and effective radii of bulges, discs and bars in [Kruk et al. \(2018\)](#) to those present in the aggregate models. We see strong consistency in all effective radii, with one major outlier, caused by the bulge growing to model the disk. There is more scatter in component axis ratio,

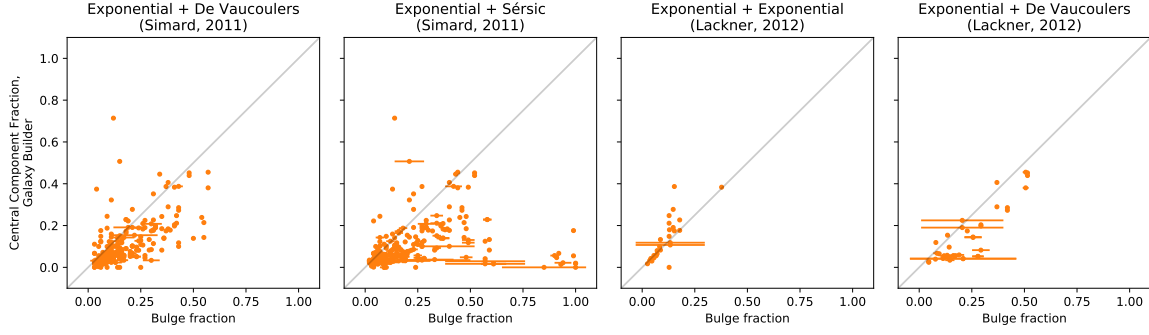


Figure 10. Scatter plots comparing the ratio of flux from central components (bulge and bar) to the total flux between fit models from *Galaxy Builder* and two-component models in the literature.

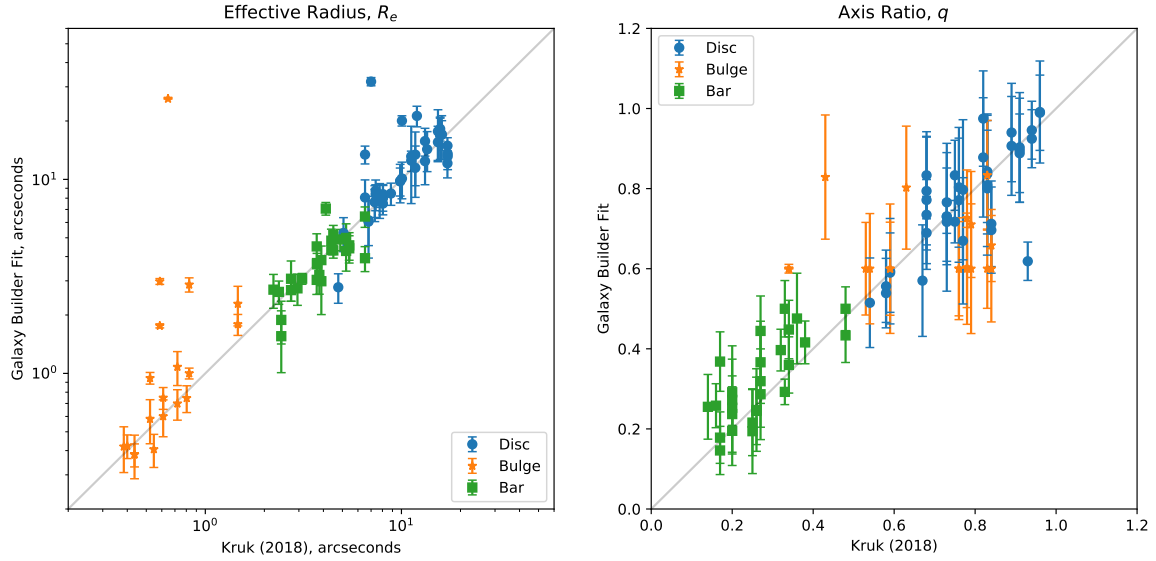


Figure 11. Comparison between *Galaxy Builder* fit models and the result of 3-component, multiwavelength fits performed by Kruk et al. (2018). Discs, Bulges and Bars are shown as blue circles, orange stars and green squares respectively. The left panel compares component effective radius, the right panel compares the component axis ratio.

with many bulges reaching the imposed lower boundary. Comparing values for central component fraction as above, we see a near-identical 1:1 relationship.

3.3.5. Comparison to Disc-Bulge-Bar-Spiral models

To the best of our knowledge, no photometric models exist for the *Galaxy Builder* sample which contain spiral arm structure. The closest comparable result is that produced by Gao & Ho (2017), however the galaxies they used are not in the Sloan footprint.

In order to provide a comparison for our novel method of spiral parameter (pitch angle and amplitude) extraction, we compare the result of our galaxy length-weighted pitch angles to the relationship obtained by Hart et al. (2016) between GZ2 classification and galaxy pitch angle. Their fit was obtained by using the Zooniverse to filter good vs bad spiral arm segments identified using an automated spiral arm detection and fitting tool, SPARCFIRE (Davis & Hayes 2014), whereas *Galaxy Builder* asks volunteers to provide their own opinion on spiral arm number, location and tightness. *Galaxy Builder* pitch angles are within the (large) uncertainties on the Hart et al. (2016) fit.

Many researches (Davis & Hayes 2014, Díaz-García et al. 2019 to name a few) have noted that many galaxies show large inter-arm variations in pitch angle, suggesting that obtaining a single value of a galaxy’s pitch angle is highly dependent on which arms have been identified. We plan to further explore this issue in a future work.

4. SUMMARY AND CONCLUSIONS

In this paper we present a novel method for modelling of galaxy images, *Galaxy Builder*, which was conceived with the goal of solving the “quality of quantity” dilemma facing galaxy image modelling, which, despite advances in computation, still typically requires significant human interaction to achieve quality fits.

Galaxy Builder leverages the power of crowd sourcing for the hardest to automate parts of image fitting, namely determining the appropriate number of model components to include, and finding regions of parameter space close to the global optima.

The use of a small sample of synthetic images to calibrate and test our model clustering and fitting code has demonstrated our ability to recover galaxy morphology, despite a systematic tendency to incorporate more bulges and fewer bars than necessary for the photometric model. As most spiral galaxies contain some form of bulge these Type 1 errors are excusable, however future work should implement an improved clustering algorithm (and improved user interface) to address the bar clustering failures present in this work. Our fitting method is still subject to the limitations of gradient-descent based optimization, for parameters for which clustering provides no prior information (bulge and bar Sérsic n , bar boxyness).

We have demonstrated our ability to obtain physically motivated models with comparable reduced chi-squared values (between 1 and 5) to results in the literature. We obtain errors on parameters where possible through the sample standard deviation of component clusters, which is less likely to be an under-estimate than Hessian approximations.

We compare these new models to existing results in the literature. We find good agreement where the models or parameters are comparable, and comment on instances where *Galaxy Builder* should provide superior models.

We were able to obtain models for 296 images with a rate of one galaxy per day. We note that user experience and task simplification will need to be considered if significantly larger numbers of these models are to be obtained. We note that, at the time of writing and to the best of our knowledge, the number of photometric models obtained here is significantly larger than the largest sample obtained through purely computational photometric fitting of disc, bulge, bar and spiral arms in galaxies (10 galaxies, Gao & Ho 2017, who also included rings, disc-breaks and further components).

We are optimistic about the potential of projects like *Galaxy Builder* to dramatically increase the ability of researchers to perform complex, labour-intensive modelling of galaxy photometry, leveraging the power of the crowd to perform the complex tasks best suited to humans, and computer algorithms for the final optimization.

We release our catalogue of models to the community, and in future work we use this sample to investigate spiral arm formation mechanisms.

5. ACKNOWLEDGEMENTS

This publication made use of SDSS-I/II data. Funding for the SDSS and SDSS-II was provided by the Alfred P. Sloan Foundation, the Participating Institutions, the National Science Foundation, the U.S. Department of Energy, the National Aeronautics and Space Administration, the Japanese Monbukagakusho, the Max Planck Society, and the Higher Education Funding Council for England. The SDSS Web Site is <http://www.sdss.org/>.

Montage is funded by the National Science Foundation under Grant Number ACI-1440620, and was previously funded by the National Aeronautics and Space Administration’s Earth Science Technology Office, Computation Technologies Project, under Cooperative Agreement Number NCC5-626 between NASA and the California Institute of Technology.

This project was partially funded by a Google Faculty Research Award to Karen Masters (<https://ai.google/research/outreach/faculty-research-awards/>), and Timothy Lingard acknowledges studentship funding from the Science and Technology Facilities Council (ST/N504245/1).

APPENDIX

A. STACKING OF MULTIPLE SDSS FRAMES

All data required for sigma image creation for stacked frames came from the corrected frames, as detailed in the frame datamodel⁹. For each pixel in an SDSS frame, we have

$$\frac{I}{C} = \frac{n}{g} - S + V, \quad (\text{A1})$$

where I represents the sky-subtracted, corrected image (nanomaggies), C represents the calibration image, n is the number of electrons captured, g is the gain, S is the Sky value (data units) and V is the dark current, $V = 0\sqrt{v}$ (v being the dark variance).

Given Poisson error,

$$\sigma_n = \sqrt{n}. \quad (\text{A2})$$

If we stack multiple frames, given N observations of a pixel

$$\begin{aligned} n_{\text{total}} &= \sum_i n_i = \sum_i g_i \left(\frac{I_i}{C_i} + S_i - V_i \right), \\ &= \sum_i \frac{g_i}{C_i} I_i + \sum_i g_i (S_i - V_i) = \sigma_{n_{\text{total}}}^2. \end{aligned} \quad (\text{A3})$$

This is ideal, and is the level that many fitting software packages work at. As we wish to return to working in units of nanomaggies on a stacked image, further calculation is needed:

$$I = \frac{1}{N} \sum_i I_i, \quad (\text{A4})$$

$$I = \frac{1}{N} \sum_i C_i \left(\frac{n_i}{g_i} - S_i + V_i \right), \quad (\text{A5})$$

And so

$$\sigma_I^2 = \frac{1}{N^2} \sum_i \frac{C_i^2}{g_i^2} \sigma_{n_i}^2 + \frac{1}{N^2} \sum_i C_i^2 \sigma_{S_i}^2 + \frac{1}{N^2} \sum_i C_i^2 \sigma_{V_i}^2. \quad (\text{A6})$$

We treat the sky value as a constant, such that $\sigma_{S_i}^2 = 0$. Substituting $\sigma_{n_i}^2 = n_i$ as above gives

$$\sigma_I^2 = \frac{1}{N^2} \sum_i \frac{C_i^2}{g_i^2} n_i + \frac{1}{N^2} \sum_i C_i^2 v_i. \quad (\text{A7})$$

$$\sigma_I = \frac{1}{N} \sqrt{\sum_i C_i^2 \left(\frac{n_i}{g_i^2} + v_i \right)}. \quad (\text{A8})$$

Note that this is identical to saying

$$\sigma_I^2 = \frac{1}{N^2} \sum_i \sigma_{I_i}^2. \quad (\text{A9})$$

B. MODEL FITTING

Assume Normal priors on component parameters determined from clustering (μ_x, μ_y, q, Re), with the spread given by the spread in the clustered values. We therefore have that our final log-likelihood (to be maximised) is the sum of the gaussian log-likelihood of the residuals given the pixel uncertainty and the gaussian log-likelihood of the variation in parameters, given their uncertainty.

⁹ https://data.sdss.org/datamodel/files/BOSS_PHOTOOBJ/frames/RERUN/RUN/CAMCOL/frame.html#example

The model being rendered is the PSF-convolved sum of the separate components and outputs an (N_x, N_y) image. The disc, bulge and bar are variations on the boxy Sérsic profile:

$$I_{\text{seraic}}(\vec{P}) = I_e \exp \left\{ -b_n \left[\left(\frac{r(\vec{P})}{R_e} \right)^{1/n} - 1 \right] \right\} \quad (\text{B10})$$

where

$$r(\vec{P}) = \left| \begin{pmatrix} \frac{1}{q} & 0 \\ 0 & 1 \end{pmatrix} \begin{pmatrix} \cos \psi & -\sin \psi \\ \sin \psi & \cos \psi \end{pmatrix} (\vec{\mu} - \vec{P}) \right|_c. \quad (\text{B11})$$

The disc is restricted to $n = 1; c = 2$, bulge to $n \in (0.5, 6); c = 2$ and bar to $n \in (0.5, 6); c \in (0.5, 6)$.

The Sérsic components are actually rendered at 5x the image resolution, and downsampled using the mean pixel brightness. This is a widely used method of approximating the true pixel value, which is an integration over the area of sky inside the pixel. I.e. for a pixel of size (δ_x, δ_y)

$$I_{\text{pix}}(\vec{P}) = \frac{1}{\delta_x \delta_y} \int_{-\delta_y/2}^{\delta_y/2} \int_{-\delta_x/2}^{\delta_x/2} dx dy I_{\text{seraic}} \left(\vec{P} + \begin{pmatrix} \delta_x \\ \delta_y \end{pmatrix} \right). \quad (\text{B12})$$

Spiral arms were restricted to be logarithmic with respect to the inclined, rotated disc. They were rendered in a similar manner to the online interface; using the nearest distance from a pixel to a calculated logarithmic spiral.

An inclined, rotated log spiral requires parameters brightness I_s , spread s , minimum and maximum θ (a and b), an amplitude A , pitch angle ϕ , position $\vec{\mu}$, position angle ψ and axis ratio q , where $\vec{\mu}$, ψ and q are inherited from the disc component.

The distance from a pixel to a logarithmic spiral is given by

$$D_s(\vec{P}) = \min_{\theta \in [a, b]} \left\| \vec{P} - \vec{\mu} - A e^{\theta \tan \phi} \begin{pmatrix} \cos \psi & \sin \psi \\ -\sin \psi & \cos \psi \end{pmatrix} \begin{pmatrix} q \cos \theta \\ \sin \theta \end{pmatrix} \right\|^2. \quad (\text{B13})$$

In practise the spiral distance was approximated using the distance to a poly-line with 200 vertices, as solving the above minimization for each pixel at each fitting step is computationally intractable. We also adjust A , a and b to account for the rotation of the disc component from its starting value, in order to prevent spirals inadvertently moving far from starting locations for face-on discs (which have poorly constrained position angles). These adjustments are

$$\begin{aligned} A' &= A e^{\Delta \psi \tan \phi}, \\ a' &= a - \Delta \psi, \\ b' &= b - \Delta \psi. \end{aligned} \quad (\text{B14})$$

The pixel brightness is then calculated as

$$I_{\text{spiral}}(\vec{P}) = I_{\text{disc}}(\vec{P}) \times I_s \exp \left(\frac{-D_s(\vec{P})}{2s^2} \right). \quad (\text{B15})$$

For the fit, we parametrize disc I_e as the Sérsic total luminosity, given by

$$L_{\text{tot}} = I_e R_e^2 2\pi n \frac{e^{b_n}}{(b_n)^{2n}} \Gamma(2n). \quad (\text{B16})$$

Bulge (bar) I_e is reparametrized as “bulge (bar) fraction”, which we define as

$$F_{\text{bulge}} = \frac{L_{\text{bulge}}}{L_{\text{disc}} + L_{\text{bulge}}}, \quad (\text{B17})$$

and is limited to be between 0 and 1. Disc luminosity is allowed to take any value greater than or equal to zero.

Similarly, bulge and bar effective radius are reparametrized as their scale relative to the disc ($R_e = R_e / R_{e, \text{disc}}$). Bulge and bar are also restricted to have the same poition.

Table 2. The maximum, minimum and default values for model parameters. Note that some parameters were allowed to overflow when fitting, for instance an axis ratio greater 1 (signifying a swap of major and minor axis) was allowed, and corrected for once fitting reached completion. This helped avoid the optimizer encountering parameter bounds and failing to converge. Component roll and spiral pitch angle was similarly unconstrained.

Component	Parameter	Tuning Minimum Bound	Tuning Maximum Bound
disc	μ_x	-inf	inf
	μ_y	-inf	inf
	roll	-inf	inf
	q	0.25	1.2
	R_e	0	inf
	Σ_e	0	inf
bulge	μ_x	-inf	inf
	μ_y	-inf	inf
	roll	-inf	inf
	q	0.6	1.2
	R_e/R_{disc}	0.01	1
	$(B/T)_r$	0	0.99
bar	n	0.5	5
	μ_x	-inf	inf
	μ_y	-inf	inf
	roll	-inf	inf
	q	0.05	0.5
	R_e/R_{disc}	0.05	1
spiral	$(B/T)_r$	0	0.99
	n	0.3	5
	c	1	6
	Σ_e	0	inf
	spread	0	inf
	ϕ	-85	85

C. ANCILLARY TABLES

REFERENCES

- Abazajian, K. N., Adelman-McCarthy, J. K., Agüeros, M. A., et al. 2009, *ApJS*, 182, 543, doi: [10.1088/0067-0049/182/2/543](https://doi.org/10.1088/0067-0049/182/2/543)
- Albareti, F. D., Allende Prieto, C., Almeida, A., et al. 2017, *ApJS*, 233, 25, doi: [10.3847/1538-4365/aa8992](https://doi.org/10.3847/1538-4365/aa8992)
- Astropy Collaboration, Price-Whelan, A. M., Sipőcz, B. M., et al. 2018, *AJ*, 156, 123, doi: [10.3847/1538-3881/aabc4f](https://doi.org/10.3847/1538-3881/aabc4f)
- Bamford, S. P., Häußler, B., Rojas, A., & Borch, A. 2011, in *Astronomical Society of the Pacific Conference Series*, Vol. 442, *Astronomical Data Analysis Software and Systems XX*, ed. I. N. Evans, A. Accomazzi, D. J. Mink, & A. H. Rots, 479
- Bertin, E., & Arnouts, S. 1996, *A&AS*, 117, 393, doi: [10.1051/aas:1996164](https://doi.org/10.1051/aas:1996164)
- Blanton, M. R., Kazin, E., Muna, D., Weaver, B. A., & Price-Whelan, A. 2011, *AJ*, 142, 31, doi: [10.1088/0004-6256/142/1/31](https://doi.org/10.1088/0004-6256/142/1/31)
- Boonchoo, T., Ao, X., & He, Q. 2018, *CoRR*, abs/1801.06965. <https://arxiv.org/abs/1801.06965>
- Bradbury, J., Frostig, R., Hawkins, P., et al. 2018, *JAX: composable transformations of Python+NumPy programs*, 0.1.55. <http://github.com/google/jax>
- Breunig, M. M., Kriegel, H.-P., Ng, R. T., & Sander, J. 2000, in *Proceedings of the 2000 ACM SIGMOD International Conference on Management of Data*, SIGMOD '00 (New York, NY, USA: ACM), 93–104, doi: [10.1145/342009.335388](https://doi.org/10.1145/342009.335388)

- Byrd, R., Lu, P., Nocedal, J., & Zhu, C. 1995, *SIAM Journal on Scientific Computing*, 16, 1190, doi: [10.1137/0916069](https://doi.org/10.1137/0916069)
- Davis, D. R., & Hayes, W. B. 2014, *ApJ*, 790, 87
- de Vaucouleurs, G., de Vaucouleurs, A., Corwin, Jr., H. G., et al. 1991, *Third Reference Catalogue of Bright Galaxies. Volume I: Explanations and references. Volume II: Data for galaxies between 0^h and 12^h. Volume III: Data for galaxies between 12^h and 24^h.*
- Díaz-García, S., Salo, H., Knapen, J. H., & Herrera-Endoqui, M. 2019, arXiv e-prints, arXiv:1908.04246. <https://arxiv.org/abs/1908.04246>
- Dobbs, C., & Baba, J. 2014, *Publ. Astron. Soc. Aust.*, 31
- Gadotti, D. A. 2011, *MNRAS*, 415, 3308, doi: [10.1111/j.1365-2966.2011.18945.x](https://doi.org/10.1111/j.1365-2966.2011.18945.x)
- Gao, H., & Ho, L. C. 2017, *ApJ*, 845, 114, doi: [10.3847/1538-4357/aa7da4](https://doi.org/10.3847/1538-4357/aa7da4)
- Gao, H., Ho, L. C., Barth, A. J., & Li, Z.-Y. 2018, *ApJ*, 862, 100, doi: [10.3847/1538-4357/aacdac](https://doi.org/10.3847/1538-4357/aacdac)
- Hart, R. E., Bamford, S. P., Willett, K. W., et al. 2016
- Hart, R. E., Bamford, S. P., Hayes, W. B., et al. 2017, *MNRAS*, 472, 2263, doi: [10.1093/mnras/stx2137](https://doi.org/10.1093/mnras/stx2137)
- Head, J. T. C. G., Lucey, J. R., & Hudson, M. J. 2015, *MNRAS*, 453, 3729, doi: [10.1093/mnras/stv1662](https://doi.org/10.1093/mnras/stv1662)
- Holincheck, A. J., Wallin, J. F., Borne, K., et al. 2016
- Hopkins, P. F., Croton, D., Bundy, K., et al. 2010, *The Astrophysical Journal*, 724, 915
- Jacob, J. C., Katz, D. S., Berriman, G. B., et al. 2010, arXiv e-prints, arXiv:1005.4454. <https://arxiv.org/abs/1005.4454>
- Jones, E., Oliphant, T., Peterson, P., et al. 2001, *SciPy: Open source scientific tools for Python*. <http://www.scipy.org/>
- Kormendy, J., Drory, N., Bender, R., & Cornell, M. E. 2010, *The Astrophysical Journal*, 723, 54
- Kruk, S. J., Lintott, C. J., Simmons, B. D., et al. 2017, *MNRAS*, 469, 3363, doi: [10.1093/mnras/stx1026](https://doi.org/10.1093/mnras/stx1026)
- Kruk, S. J., Lintott, C. J., Bamford, S. P., et al. 2018, *MNRAS*, 473, 4731, doi: [10.1093/mnras/stx2605](https://doi.org/10.1093/mnras/stx2605)
- Lackner, C. N., & Gunn, J. E. 2012, *MNRAS*, 421, 2277, doi: [10.1111/j.1365-2966.2012.20450.x](https://doi.org/10.1111/j.1365-2966.2012.20450.x)
- Lange, R., Moffett, A. J., Driver, S. P., et al. 2016, *MNRAS*, 462, 1470, doi: [10.1093/mnras/stw1495](https://doi.org/10.1093/mnras/stw1495)
- Lintott, C. J., Schawinski, K., Slosar, A., et al. 2008, *Monthly Notices of the Royal Astronomical Society*, 389, 1179
- Lupton, R., Blanton, M. R., Fekete, G., et al. 2004, *PUBL ASTRON SOC PAC*, 116, 133
- Masters, K. L., & the Galaxy Zoo Team. 2019, arXiv e-prints, arXiv:1910.08177. <https://arxiv.org/abs/1910.08177>
- Masters, K. L., Nichol, R. C., Hoyle, B., et al. 2010, *Monthly Notices of the Royal Astronomical Society*, 411, 2026
- Mendez-Abreu, J., Ruiz-Lara, T., Sanchez-Menguiano, L., et al. 2016
- Park, C., Choi, Y.-Y., Vogeley, M. S., et al. 2007, *ApJ*, 658, 898
- Pedregosa, F., Varoquaux, G., Gramfort, A., et al. 2011, *Journal of Machine Learning Research*, 12, 2825
- Peng, C. Y., Ho, L. C., Impey, C. D., & Rix, H.-W. 2002, *AJ*, 124, 266, doi: [10.1086/340952](https://doi.org/10.1086/340952)
- . 2010, *AJ*, 139, 2097, doi: [10.1088/0004-6256/139/6/2097](https://doi.org/10.1088/0004-6256/139/6/2097)
- Pour-Imani, H., Kennefick, D., Kennefick, J., et al. 2016, *The Astrophysical Journal*, 827, L2
- Pozzetti, L., Bolzonella, M., Zucca, E., et al. 2009, *Astronomy & Astrophysics*, 523, A13
- Robotham, A. S. G., Taranu, D. S., Tobar, R., Moffett, A., & Driver, S. P. 2016
- Salo, H., Laurikainen, E., Laine, J., et al. 2015, *ApJS*, 219, 4, doi: [10.1088/0067-0049/219/1/4](https://doi.org/10.1088/0067-0049/219/1/4)
- Sanchez, S. F., Kennicutt, R. C., de Paz, A. G., et al. 2011, *Astronomy and Astrophysics*, 538, A8
- Simard, L., Mendel, J. T., Patton, D. R., Ellison, S. L., & McConnachie, A. W. 2011, *ApJS*, 196, 11, doi: [10.1088/0067-0049/196/1/11](https://doi.org/10.1088/0067-0049/196/1/11)
- Simard, L., Willmer, C. N. A., Vogt, N. P., et al. 2002a, *ASTROPHYS J SUPPL S*, 142, 1
- . 2002b, *The Astrophysical Journal Supplement Series*, 142, 1
- Simmons, B. D., Lintott, C., Willett, K. W., et al. 2017, *MNRAS*, 464, 4420, doi: [10.1093/mnras/stw2587](https://doi.org/10.1093/mnras/stw2587)
- Simpson, R., Page, K. R., & De Roure, D. 2014, in *Proceedings of the 23rd International Conference on World Wide Web, WWW '14 Companion* (New York, NY, USA: ACM), 1049–1054, doi: [10.1145/2567948.2579215](https://doi.org/10.1145/2567948.2579215)
- Stoughton, C., Lupton, R. H., Bernardi, M., et al. 2002, *AJ*, 123, 485, doi: [10.1086/324741](https://doi.org/10.1086/324741)
- Vika, M., Bamford, S. P., Häußler, B., & Rojas, A. L. 2014, *Monthly Notices of the Royal Astronomical Society*, 444, 3603
- Willett, K. W., Lintott, C. J., Bamford, S. P., et al. 2013
- Willett, K. W., Galloway, M. A., Bamford, S. P., et al. 2017, *MNRAS*, 464, 4176, doi: [10.1093/mnras/stw2568](https://doi.org/10.1093/mnras/stw2568)
- Zaninetti, L. 2014, arXiv e-prints, arXiv:1401.0287. <https://arxiv.org/abs/1401.0287>